GRC Transactions, Vol. 40, 2016

Geothermal Field Work using a Drone with Thermal Camera: Aerial Photos, Digital Elevation Models and Heat Flow

M.C. Harvey

School of Environment, University of Auckland, Auckland, New Zealand,

Key Words:

thermal, infrared, geothermal, exploration, camera, drone, uav, rpas, New, Zealand, monitoring, photogrammetry, structure, motion, heat, flow, flux.

Corresponding author: mhar098@aucklanduni.ac.nz (+64) 21 1045 333

Key Points

- Drone captured georeferenced, temperature-calibrated thermal orthophoto of Karapiti thermal area, Wairakei, New Zealand.
- Calibrated thermal imagery and shallow gradient measurements provide an estimate of a total heat flow of 119 MW for steam heated ground in the survey area.
- Aerial photo and digital elevation model (DEM) were produced for the Karapiti geothermal area
- This study demonstrates the utility and economy of drones for producing accurate aerial photos, DEM's and thermal imagery

Abstract

Drones are now routinely used for collecting aerial imagery and creating digital elevation models (DEM). Lightweight thermal sensors provide another payload option for generation of very high resolution aerial thermal orthophotos. This technology allows for the rapid and safe survey of thermal areas, often present in inaccessible or dangerous terrain. Here we present a 0.5 km^2 georeferenced, temperature-calibrated thermal orthophoto of thermal ground within the Wairakei geothermal area, New Zealand. The image represents a mosaic of ~1000 thermal images captured by drone over a period of about 2 hours. This is probably the first such image of a significant area of steam heated ground ever produced by a drone equipped with a thermal camera. Temperature calibration of the image allowed calculation of diffuse heat flow (119 MW) from steam heated ground in the survey area (diffuse heat flow excludes fumaroles). An

Red Green Blue (RGB - visible spectrum) orthomosaic photo and digital elevation model was also produced for these areas, with ground resolution and horizontal position error comparable to commercially produced LiDAR and aerial imagery obtained from manned aircraft. Our results show that thermal imagery collected by drones has the potential to become a key tool in geothermal science, including geological, geochemical and geophysical surveys, environmental baseline and monitoring studies, geotechnical studies and civil works.

1 Introduction

Photogrammetry is a technology that allows the reconstruction of three dimensional information (i.e. Digital Elevation Models) from a mosaic of overlapping, two dimensional photographs (Westoby et al., 2012). Although photogrammetry is not a new technology, recent advances in Unmanned Aerial Vehicle (UAV or drones) equipped with global positioning systems (GPS) and digital cameras have reduced the cost of collecting imagery. Modern desktop and cloud computing power allows for routine post processing of large numbers of individual image photos. The individual photos are combined into aerial orthophotos and Digital Elevation Models (DEM) of comparable quality (<0.1m) to airborne LiDAR (Harwin & Lucieer, 2012; Fonstad et al., 2013).

Lightweight thermal sensors provide another payload option for generation of very high resolution aerial thermal orthophotos. This technology promises to allow the rapid, safe and cost-effective survey of thermal areas, often present in inaccessible or dangerous terrain.

In this study we provide results from a thermal infrared and Red Green Blue (RGB) survey of the Karapiti thermal area, located within the Wairakei geothermal system, New Zealand. The survey was undertaken using a drone equipped with a point and shoot digital camera for standard visible images (RGB), and a thermal infrared camera. Heat flux in the survey area was also assessed by ground temperature profile measurements.

The Karapiti survey area comprises widespread (~0.5 km^2) steam heated ground and fumaroles; the surface expression of a rhyolite dome that penetrates the Huka Falls mudstone (local caprock). The dome allows steam to escape through near-surface permeable ash and pumice (Rosenberg et al., 2009). The purpose of this study was to assess the usefulness of drone technology for mapping steam heated ground, and to provide an estimate of heat flow for the survey area.

2 Methods

2.1 Field Methods

Imagery was collected using a modified DJI Phantom 2 Vision plus quadcopter (Figure 1). The quadcopter was modified by the replacement of the stock camera with an ICI 640x480 uncooled thermal sensor (spectral response 7-14µm) with automated image capture (ICI UAV module®). A Canon S100 point and shoot camera was fitted for normal visible (RGB) and DEM outputs (Harvey et al., 2014). Both camera systems automatically geotag images which provides georeferenced output.

Figure 1 DJI Phantom 2 Vision Plus quadcopter modified with ICI thermal camera and UAV module

An appropriate flight plan was determined using UgCS® software running on a Hewlett Packard laptop running Windows 7®. The flight plan was then uploaded to the quadcopter's flight controller via a Samsung S4 smartphone running Android and the UgCS® mobile companion App. Accordingly, both in-flight navigation and image capture were autonomous.

Calibration of the thermal imagery was by direct measurement of water on the ground using a Type-K thermocouple temperature probe; measurement of hot and cold pools (farm troughs) allowed raw pixel response values from the thermal camera to be calibrated for a range of ambient conditions.

In addition to thermal infrared imagery, heat flux in the survey area was assessed by the methods of Hochstein and Bromley (2005), based on shallow ground temperature measurements. Measurement locations were regularly spaced (~50m, *Figure 5*) within the survey area to avoid

clustering bias. Temperature was measured at 10cm intervals using a handheld Type K thermocouple probe inserted to a maximum depth of 1m below ground level. Temperature was measured at 5 cm intervals in certain locations with very high heat flow so depth to boiling point to could be more accurately measured (i.e. where depth to boiling point was <20cm). The probe temperature was allowed to equilibrate for at least 30 seconds before each reading. Two probes were carried to allow cross checking of temperature measurements to verify measurement accuracy.

2.2 Image Processing and Analysis

Two-dimensional Thermal and RGB images were converted to 3-dimensional point clouds using Agisoft Photoscan® commercial photogrammetry software, running on a Hewlett Packard laptop computer equipped with an i7 processor and 32GB RAM. Processing provided georeferenced, thermal and RGB raster orthophotos, and a DEM (*Table 1*).

Raster imagery was analysed and post-processed using QGIS open-source desktop geographic information system (GIS). Post processing steps included conversion of the raw pixel values to calibrated temperature values (°C), and then to heat flux values (W m^{-2}), as described below.

2.3 Calculation of Heat Flow

Areas of barren thermal clay (*Figure 5*) were selected from the temperature calibrated raster image using the SCP plugin for QGIS. For this purpose, the QGIS Raster Calculator tool was used to firstly select pixels above an appropriate temperature threshold (20°C), then calculate the

heat flux Q_{tot} (W m^{-2}) for selected pixels, by applying empirical formulae of Bromley et al. (2011):

$$Q_{tot} = 50.3\ (T_s - T_{amb}) - 148 \qquad (1)$$

Where:

T_s = calibrated pixel temperature value (°C)

T_{amb} = ambient surface temperature (°C)

Heat flow (W) was obtained for each pixel by multiplication with the pixel area (0.056 m^2), and pixels summed to give total heat flow for the barren clay area.

The remainder of the above-background thermal area (12 – 20°C) selected by the QGIS Raster Calculator was covered in thermal vegetation, mostly Prostrate Manuka (*Figure 5*). The above approach to estimate heat flow (*Eq. 1*) was tried in this area but provided a very low estimate (compared to the ground based shallow temperature gradient method). Probably because the vegetation was insulating the ground (i.e. low pixel values). Accordingly, heat flow was estimated as the product of i) the average heat flux (300 W m^{-2}) of temperature gradient measurements within the area (n = 69), and ii) the area (m^2) of all pixels in this area.

Heat flux from shallow gradient measurements was assessed using the empirical function of Hochstein and Bromley (2005). This function is based on the depth of boiling and uses an

average heat flux of 185 W m^{-2} (α) alongside an empirical constant, β, of 0.757. This equation provides the total heat flux per m^2, incorporating both convective and conductive processes.

$$Q_{tot} = \alpha (Z_{bp}/Z_o)^{-\beta} \qquad (2)$$

Where Q_{tot} is the total heat flux per m^2, α is 185 W m^{-2}, β is an empirically derived constant, 0.757, Z_{bp} is the depth to boiling, and Z_o is the unit of depth (1 m).

If the boiling point depth was not reached, it was obtained by extrapolation assuming a power law or polynomial relationship, whichever gave the best curve fit.

3 Results

For thermal imagery, 4 flights were made between 0600 and 0800 on the 2nd April 2016. Flight conditions were clear and cool (12°C) in the early morning, with light winds ~1 m/s. The total flight time was about 30 min, providing 1026 thermal images. Computer post-processing of imagery took about 2 hours, providing a thermal orthophoto with a total coverage of ~0.5 km^2 and ground resolution of 19 cm (*Figure 2*)(*Table 1*). Manual cross checking alignment of the thermal orthophoto with the visible orthophoto indicates positional error for the majority of the thermal image is <1 m (offset from the visible orthophoto). Steam heated ground is clearly identifiable in the thermal orthophoto (*Figure 2*).

Calibration of the thermal image showed a linear pixel response to measured temperatures, however increased scatter was observed at higher temperatures (>80°C). A linear equation was

fitted to the calibration scatter plot ($r^2 = 0.98$), which allows temperature to be estimated for each pixel (±2.3 °C for T<80°C) (*Figure 6*). *Figure 5* illustrates the selection of pixels for a chosen temperature interval using the QGIS Raster Calculator tool (2.3).

Calibrated thermal imagery provided a total heat flow of 15 MW for thermal clays (>20°C) in the survey area (0.03 km^2). The larger vegetated area (0.35 km^2) provided a total heat flow of 104 MW (*Table 2*), based on the thermal imagery and ground-based temperature gradient measurements.

Table 1 Image processing output

Description	Ground Resolution (m)	RMS Error (m)	Area (km^2)	Computer Processing Time (hours)
Temperature calibrated thermal orthophoto	0.19	~1 (x), ~1 (y)	0.5	2
Georeferenced RGB orthophoto	0.04	0.7 (xy)	0.8	6
Georeferenced DEM	0.17	0.7 (xy), 1.6(z)	0.8	-

Table 2 Karapiti heat flux

Area	Surface Temp (°C)	Area (m^2)	Mean Heat Flux ($W\ m^{-2}$)	Total Heat Flow (MW)
Thermal Clay	>20	34315	450	15
Thermal Vegetation	12-20	346110	300	104
Total		**380425**		**119**

For the visible imagery and the DEM, 2 flights were made at midday, 29th April 2016. Flight conditions were clear and sunny, with maximum wind speed of ~4 m/s. The total flight time was about 20 minutes, providing 672 images. Computer post-processing of imagery took about 6 hours, providing an orthophoto and DEM with a total coverage of ~0.8 km^2, and orthophoto

ground resolution of 4 cm (*Figure 3* - *Figure 4*) (*Table 1*). Ground control check points provided Root Mean Squared (RMS) positional error in the horizontal plane of 0.7 m and 1.6 m in the vertical axis.

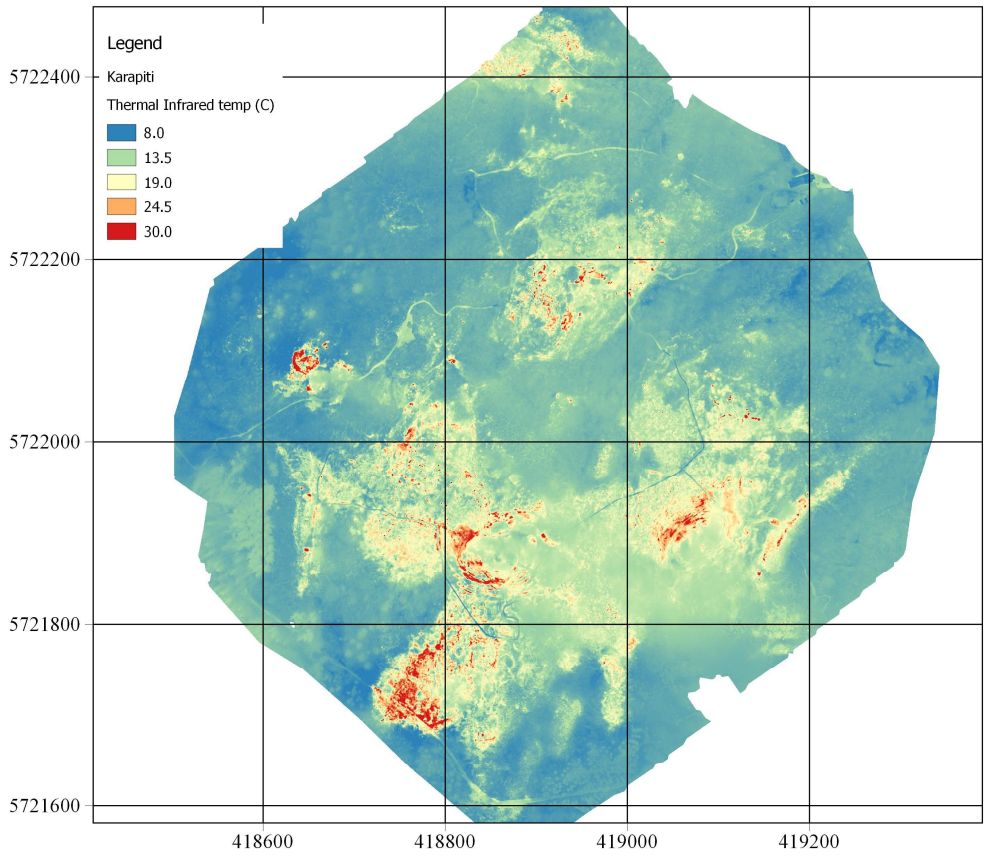

Figure 2. Karapiti calibrated thermal infrared orthophoto. Map datum WGS84.

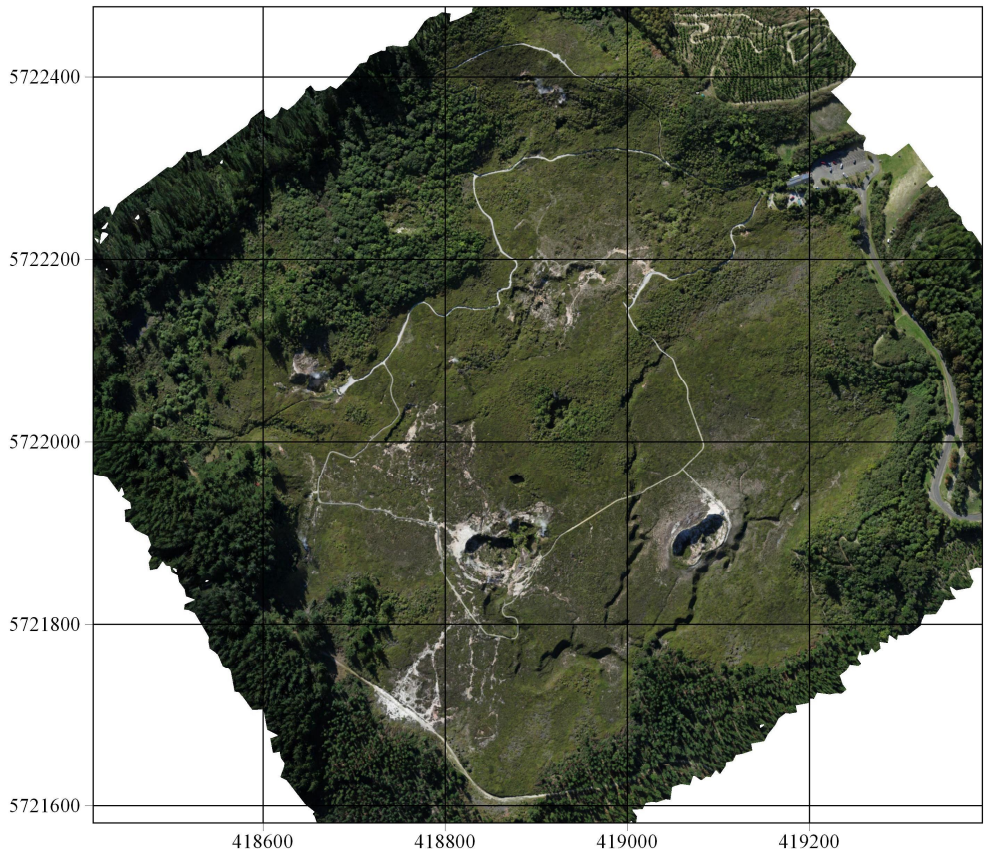

Figure 3. Karapiti RGB orthophoto. Map datum WGS84.

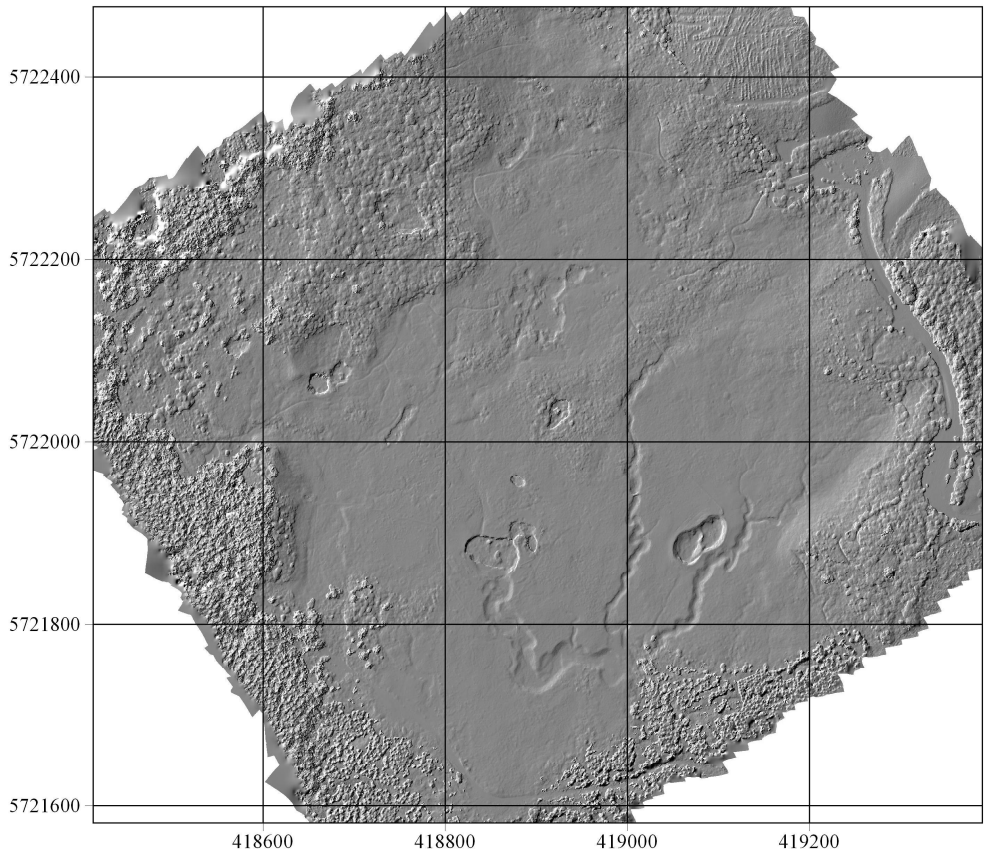

Figure 4. Karapiti digital elevation model (DEM) showing hydrothermal eruption craters. Map datum WGS84.

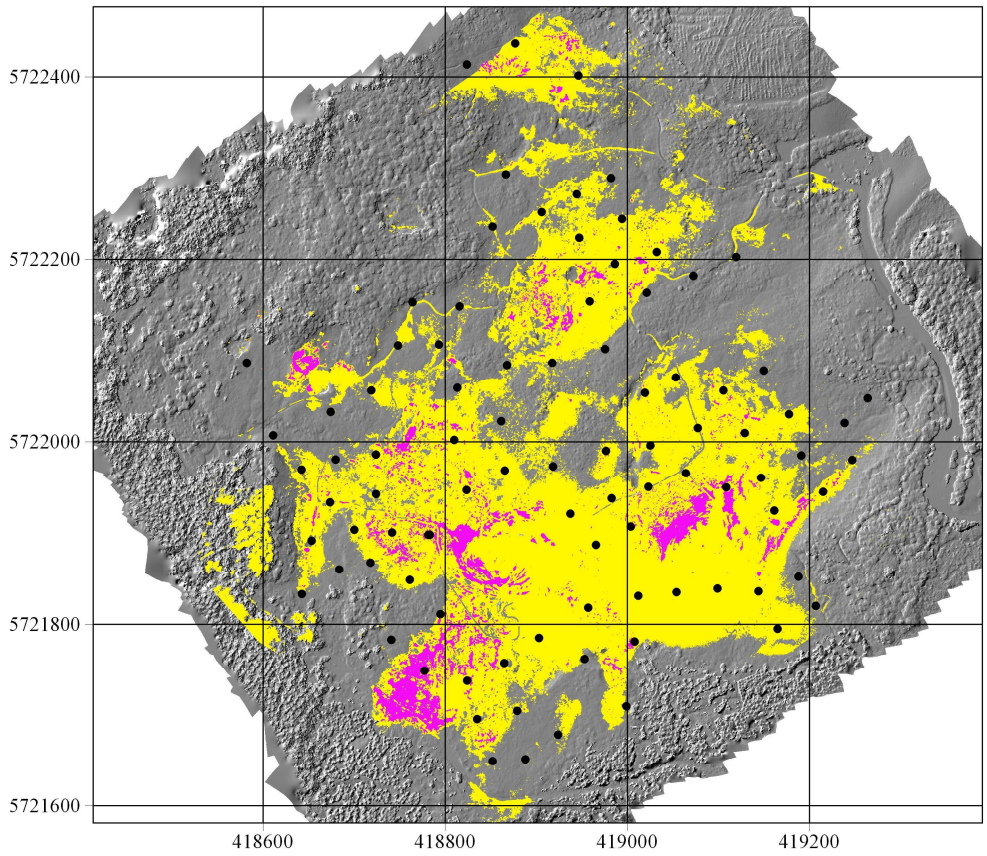

Figure 5. Areas of barren thermal clay (magenta: >20°C) and thermo-tolerant vegetation (yellow: 12-20°C) used for heat flow estimate. Black dots show locations of shallow temperature profile measurements. Map datum WGS84.

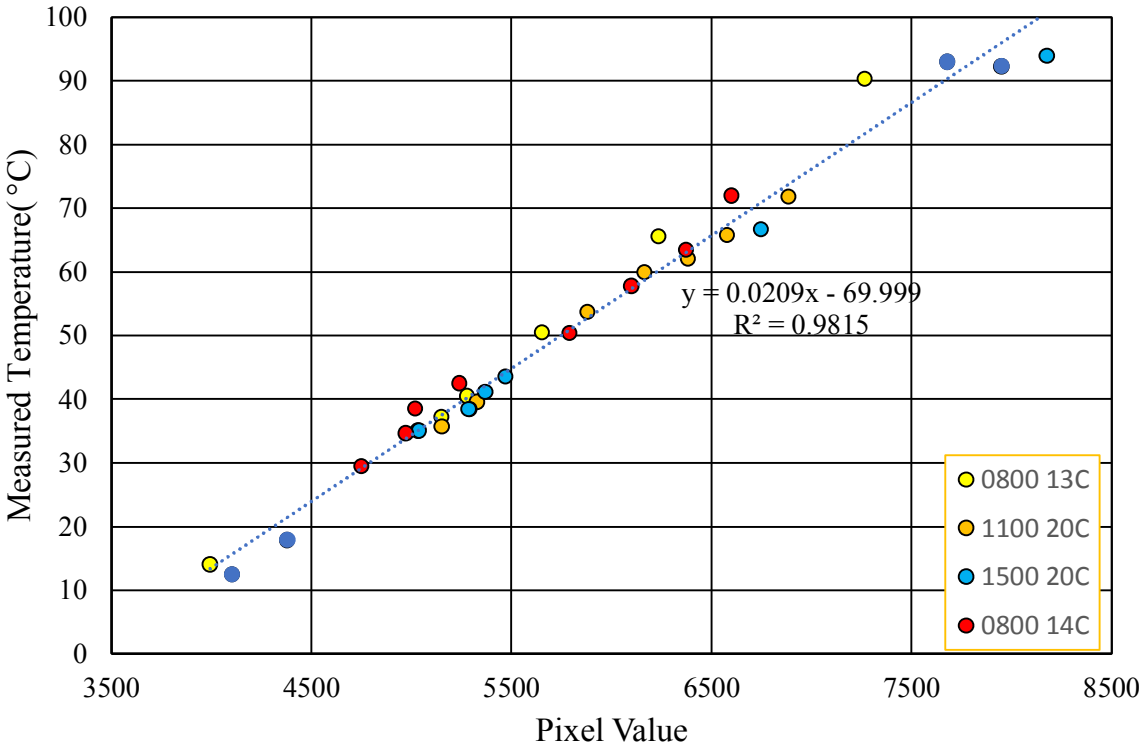

Figure 6. Thermal camera calibration. Points are colour coded according to the time of day and ambient temperature during calibration flight. Line of best fit and equation are for all points. Standard error = 2.3 °C (for measurements <80°C).

4 Discussion and Conclusions

The most significant output of this study is production of a 0.5 km^2 georeferenced, temperature-calibrated thermal orthophoto at Karapiti. The image represents a mosaic of 1026 thermal images captured by drone over a period of 2 hours. This is probably the first such image of a large steam-heated geothermal area ever produced by a drone equipped with a thermal camera. This study demonstrates there are no technical barriers preventing the use of drones to produce accurate thermal and visible maps of large, potentially inaccessible geothermal areas.

For non-thermal imagery, the ground resolution (4cm) is comparable to commercially produced LiDAR and aerial imagery obtained from crewed aircraft. The position error of the thermal orthophoto was estimated by checking alignment with the georeferenced visible image and found to <1m for most of the image area.

Thermal imagery was calibrated by ground truthing; hot and cold pools of water were measured with a Type K thermocouple. The measured pools were imaged during a series of flights made over a range of temperature conditions. The calibration cross-plot showed increased scatter at higher temperatures that may be due to interference from steam. However, the correlation in the cross plot is good ($r^2 = 0.98$), with a standard error of the regression of ± 2°C under 80°C. This has allowed the generation of calibrated and georeferenced thermal imagery that can be investigated in detail and analysed with standard GIS software (ArcGIS, QGIS, etc.).

Calibrated thermal imagery provided a total heat flow of ~15 MW for thermal clays (>20°C) in the survey area. This value is a minimum as steam partly obscured the survey area; thermal infrared radiation is absorbed by steam. A larger heat flow value would be obtained by flying later in the day, on a colder day; relative humidity increases atmospheric steam and is usually highest in the early morning then drops rapidly after sunrise. Accordingly, optimal flight conditions for thermal survey of steaming ground are probably during periods of relatively cool, dry weather, with even cloud cover, possibly around midday. However, this remains to be tested.

The larger vegetated area provided a total heat flow of 104 MW. Together, the total diffuse heat flow of 119 MW from an area of 0.38 km^2 is comparable to previous estimates derived from shallow temperature gradient measurements (138 MW) (Bromley& Hochstein, 2005), and thermal infrared imagery (~100 MW) (Bromley and Graham, 1999).

Acknowledgments

We would like to acknowledge the Craters of the Moon Trust, GNS Science, ICI Cameras and The University of Auckland.

REFERENCES

Bromley, C.J., Graham, D. (1999). Wairakei Heatflow-1997. IGNS unpublished report 1999/46 for Contact Energy.

Fonstad, M. A., Dietrich, J. T., Courville, B. C., Jensen, J. L. and Carbonneau, P. E. (2013). Topographic structure from motion: a new development in photogrammetric measurement. Earth Surf. Proc. Land, 38: 421–430. doi: 10.1002/esp.3366.

Harvey, M.C., Pearson, S., Alexander, K.B., Rowland, J. & White, P. (2014). Unmanned aerial vehicles (UAV) for cost effective aerial orthophotos and digital surface models (DSMs). New Zealand Geothermal Workshop 2014 Proceedings, Auckland, New Zealand.

Harwin S, Lucieer A. (2012). Assessing the Accuracy of Georeferenced Point Clouds Produced via Multi-View Stereopsis from Unmanned Aerial Vehicle (UAV) Imagery. Remote Sensing; 4(6):1573-1599.

Hochstein, M. P. and C. J. Bromley (2005). Measurement of heat flux from steaming ground, *Geotherm., 34*, 131-158.

Bromley, C. J., & Hochstein, M. P. (2005). Heat discharge of steaming ground at Karapiti (Wairakei), New Zealand. In *Proceedings of the World Geothermal Congress*.

Rosenberg, M. D., Bignall, G., & Rae, A. J. (2009). The geological framework of the Wairakei–Tauhara geothermal system, New Zealand. *Geothermics*, *38*(1), 72-84.

Westoby, M. J., Brasington, J., Glasser, N. F., Hambrey, M. J., & Reynolds, J. M. (2012). 'Structure-from-Motion' photogrammetry: A low-cost, effective tool for geoscience applications. Geomorphology, 179, 300-314.